Published by Avanti Publishers

Global Journal of Energy Technology Research Updates

ISSN (online): 2409-5818

Experimental Evaluation of a Simulated Geothermal Heat Pump System for Potential Large-Scale Space Heating Application at TBRHSC in Severe Cold Climate in Northwestern Ontario, Canada

Basel I. Ismail* and Anjali Nagi

Department of Mechanical & Mechatronics Engineering, Lakehead University, 955 Oliver Road, Thunder Bay, Ontario P7B5E1, Canada

ARTICLE INFO

Article Type: Research Article

Academic Editor: Saad A. El-Sayed

Keywords:
Ground temperature
Northwestern Ontario
Large-scale space heating
Clean energy technologies
Cold climate energy efficiency
Geothermal heat pump (GHP)
Ground-source thermal systems
Experimental performance evaluation

Timeline:
Received: October 01, 2025
Accepted: November 15, 2025
Published: December 09, 2025

Citation: Ismail BI, Nagi A. Experimental evaluation of a simulated geothermal heat pump system for potential large-scale space heating application at TBRHSC in severe cold climate in Northwestern Ontario, Canada. Glob J Energ Technol Res Updat. 2025; 12: 30-43.

DOI: https://doi.org/10.15377/2409-5818.2025.12.3

ABSTRACT

Space heating for buildings and institutional complexes represents a dominant sector of energy consumption and greenhouse gas (GHG) emissions in Canada, a challenge exacerbated by the nation's cold climate. This is particularly critical in regions like Thunder Bay, where harsh winters and significant heating demands make the building sector a major contributor to local emissions—the residential sector alone accounts for 27% of community GHG output. The geothermal heat pump (GHP), or ground-source heat pump, is a highly efficient technology that leverages the stable thermal energy of the subsurface to provide space conditioning. By using the ground as a heat source in winter and a heat sink in summer, GHPs can reduce heating and cooling energy use by 25–50% compared to conventional systems. This makes them a promising solution for large-scale space heating applications, such as at the Thunder Bay Regional Health Sciences Centre (TBRHSC), a major healthcare facility and one of the city's largest energy consumers. Despite this potential, there remains a significant gap in region-specific performance data and operational understanding of GHPs in extreme cold climate in Northwestern Ontario. This study addresses that gap through experimental characterization of a lab-scale GHP system using actual subsurface temperature profiles. An extensively instrumented GHP simulator was employed to evaluate system performance across a key range of operating conditions. The experimental results showed that the supply air temperature from the GHP system rises rapidly following system start-up, with each tested condition achieving approximately 90% of its peak value within the first 4 to 5 minutes. A consistent thermal gain of the GHP was observed, where each 5°C increase in entering water temperature yielded an additional 3°C rise in the useful supply air temperature. The temperature gradients plateau after 10 min indicating that the system has achieved a thermal steady state. Progressively increasing the simulated ground-loop water temperature entering the GHP's evaporator from 5°C to 10°C and then to 15°C resulted in a corresponding rise in supply hot air temperature and an improvement in the GHP system's coefficient of performance (COP).

*Corresponding Author
Email: bismail@lakeheadu.ca
Tel: +(1) 807-766-7100

©2024 Ismail and Nagi. Published by Avanti Publishers. This is an open access article licensed under the terms of the Creative Commons Attribution Non-Commercial License which permits unrestricted, non-commercial use, distribution and reproduction in any medium, provided the work is properly cited. (http://creativecommons.org/licenses/by-nc/4.0/)

1. Introduction

Escalating thermal and electrical demands, particularly in cold remote regions, coupled with stringent regulations targeting greenhouse gas (GHG) emissions and air pollution, and growing concerns over finite natural resources have intensified global interest in innovative renewable energy technologies for integrated heating, cooling, and power generation [1-3]. Geothermal energy is derived from the Greek words "geo" (earth) and "therme" (heat), refers to the thermal energy stored within the Earth's subsurface. Geothermal heat pumps (GHPs) leverage the fundamental physical principle that subsurface temperatures remain relatively stable throughout the year. This thermal stability enables a geothermal heat pump (GHP) to function efficiently in both heating and cooling modes, as the ground acts as a heat source in winter and a heat sink in summer, in contrast to more variable ambient air temperatures, like those conventionally used known as air-source heat pumps (ASHP). GHPs present a technologically attractive alternative to conventional heating, ventilation, and air conditioning (HVAC) systems due to their superior energy utilization efficiency, making them prevalent for space conditioning and water heating in buildings. There are many numerical and experimental studies on fundamentals, modeling, experimental and technical performance aspects, as well as benefits of using GHP systems for heating and cooling [4-24], more particularly when operating in extreme cold climate [5, 23]. The benefits of GHP systems are multifaceted, encompassing environmental, economic, comfort, and safety advantages. Conventional combustion-based systems, which burn fossil fuels such as natural gas (primarily methane), consume oxygen (O_2) and produce carbon dioxide (CO_2)—a primary greenhouse gas contributing to global warming and climate change—alongside other harmful pollutants. In contrast, GHP systems, which transfer rather than generate heat, produce significantly lower direct CO_2 emissions and pollutants. Consequently, this innovative clean technology is garnering increased adoption in North America and Europe for its potential to drastically reduce primary energy consumption and associated emissions. Operationally, GHPs can significantly lower long-term heating and cooling costs. They are frequently paired with low-temperature radiant floor or wall distribution systems, which promote occupant comfort and a healthy indoor climate by minimizing air temperature stratification and reducing airborne dust circulation. Furthermore, as a non-combustion thermodynamic cycle, GHP systems inherently reduce risks associated with fire and fuel-related accidents.

A heat pump is a thermodynamic device that transfers thermal energy for heating or cooling applications. Primary configurations include air-to-air, air-to-water, water-to-air, and water-to-water systems, with the water-to-air type being most common in geothermal applications [7]. System performance is quantified by the coefficient of performance (COP). A standard vapor-compression heat pump cycle comprises four key components: an evaporator, a compressor, a condenser, and an expansion valve, with R-134a being a commonly employed refrigerant [8]. A complete GHP system integrates three primary subsystems, as illustrated in Fig. (**1**), a ground-loop heat exchanger (a closed circuit of buried piping containing a heat-transfer fluid, typically an antifreeze solution), the heat pump unit itself (the closed refrigerant cycle), and an HVAC distribution system.

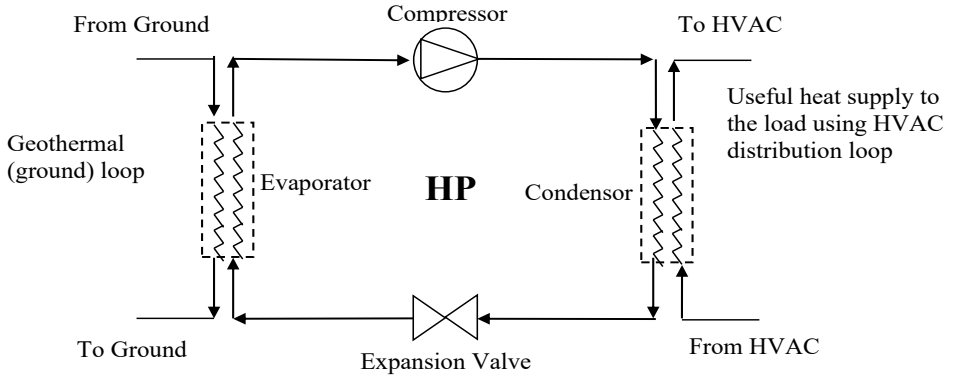

Figure 1: A schematic diagram illustrating a typical geothermal heat pump (GHP) system.

Operation involves circulating the fluid through the buried ground loop to absorb or reject heat from the earth. This thermal energy is transferred to the refrigerant at the evaporator. The refrigerant is then compressed,

elevating its temperature, before rejecting heat to the building's air (via a fan coil unit and ductwork) at the condenser, thereby providing space heating.

The Thunder Bay Regional Health Sciences Centre (TBRHSC), located in Thunder Bay, Ontario, is the principal tertiary healthcare provider for Northwestern Ontario, delivering advanced medical services across a large, dispersed population. As a hub for regional healthcare innovation and education, TBRHSC is recognized for its comprehensive specialty care in oncology, cardiology, and emergency medicine. Its extensive infrastructure, including 375 inpatient beds, necessitates continuous, high-energy operation, positioning the facility as a critical site for energy efficiency and sustainability initiatives. The hospital has established targets to reduce natural gas consumption by 5% (2025–2029) and 8% by 2035, alongside a 3% reduction in energy use intensity (EUI) within five years and 6% by 2035. These objectives support its commitment to lowering greenhouse gas (GHG) emissions by 10% from 2016 levels by 2035, consistent with Ontario's aim for a 30% reduction from 2005 levels by 2030 [9]. TBRHSC's strategic integration of energy management into daily operations prioritizes indoor environmental quality, operational efficiency, and sustainable decision-making. This proactive framework establishes an ideal context for evaluating geothermal energy solutions, which could substantially advance the hospital's energy conservation and GHG reduction goals. Implementing a renewable geothermal heating and cooling system would directly support TBRHSC's aims to decrease fossil fuel reliance, improve operational efficiency, and enhance sustainability while meeting its significant thermal demands. This analysis is crucial for assessing the potential benefits and integration challenges of geothermal heat pump (GHP) technology within TBRHSC's infrastructure, more particularly when operating in severe cold climate in Northwestern Ontario. To diminish fossil fuel dependence and reduce operating expenses, the GHP system represents a promising solution offering a highly efficient and sustainable method for meeting a building's heating and cooling requirements. An aerial photograph of TBRHSC is provided in Fig. (**2**) [25].

Figure 2: An arial view of Thunder Bay Regional Health & Science Centre (TBRHSC), Thunder Bay, Northwestern Ontario [25].

Existing research has extensively characterized the performance of geothermal heat pump (GHP) systems [17]. However, investigations that incorporate site-specific geothermal properties—such as actual ground temperature profiles derived from field measurements—remain limited for potential space heating applications more particularly in extreme cold regions such as Northwestern Ontario, Canada, where GHP could be potentially applied for the large-scale TBRHSC facility located in Thunder Bay city. These precise profiles are critical for feasibility studies, enabling accurate system assessments. Therefore, this study's primary objective is to experimentally characterize a lab-scale GHP (referred to as a GHP simulator) using actual geothermal temperature data measurement station at a nearby site (Musselwhite gold mine site) in Northwestern Ontario. Geothermal logging stations and HOBO micro-weather instrumentation were deployed at the site to collect extensive, actual subsurface temperature measurements at multiple depths across two distinct locations of boreholes at the site in the first phase of this Lakehead University Engineering-Musselwhite geothermal project (2007-2009) [26]. Data acquisition utilized ground temperature sensors and remote-radio data acquisition system. Subsequently,

comprehensive laboratory tests were conducted using a fully instrumented GHP simulator, driven by the site-specific ground thermal data. In this paper, more detailed tests were performed to evaluate the GHP simulator's performance across a wide range of operating conditions relevant to a potential future large-scale heating application for the TBRHSC health care facility. Key performance characteristics and findings from these detailed experimental simulations using the GHP simulator are presented in the following sections.

2. The Experimental GHP Simulator

In this investigation, a fully instrumented, lab-scale geothermal heat pump (GHP) simulator was designed and constructed. A comprehensive series of tests was conducted using this apparatus, accompanied by rigorous energy analysis, to elucidate system performance across a wide range of operating conditions modeled after the geothermal data acquired from the site. A photograph and schematic diagram of the GHP simulator are shown in Fig. (**3**) and Fig. (**4**), respectively.

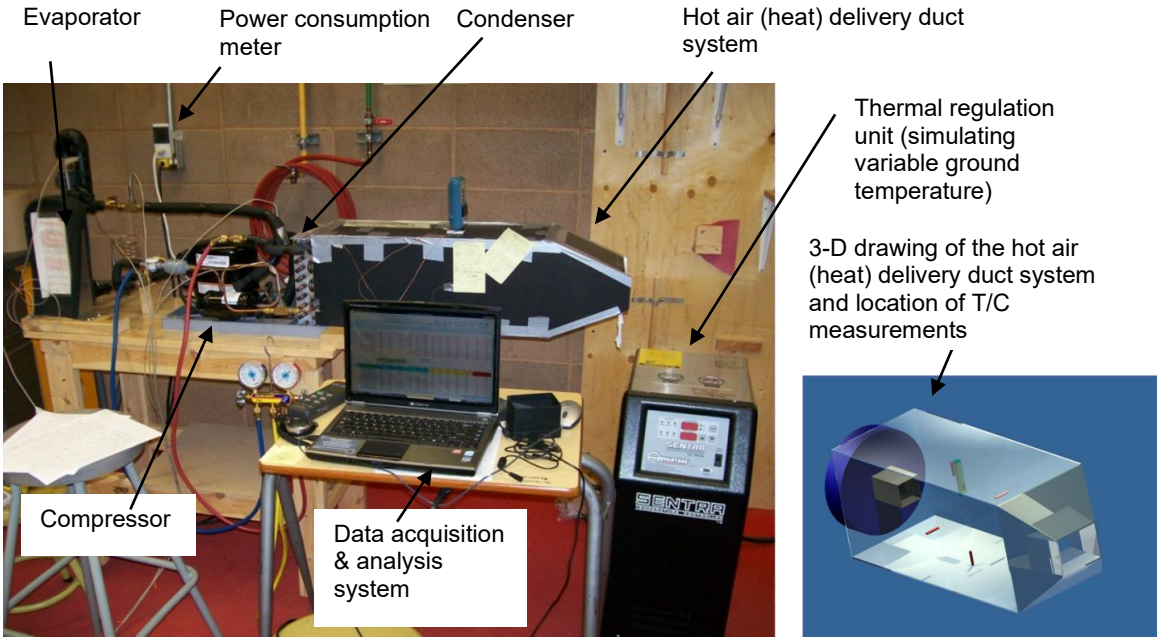

Figure 3: A photograph showing the GHP simulator used in this study**.**

As illustrated in Fig. (**4**), the experimental system is built upon two core loops: a simulated geothermal ground loop and a closed heat pump refrigerant cycle, supplemented by an integrated air duct system to replicate space heating. A plate-type heat exchanger within the GHP simulator facilitates the primary thermal energy transfer from the simulated geothermal source to the refrigerant R-134a. The inlet temperature to the heat pump was precisely controlled and varied to evaluate performance dependencies. Comprehensive instrumentation, including pressure gauges, K- and T-type thermocouples, and control valves, was installed at strategic locations across the assembly, as depicted in Fig. (**4**). The Pressure Manifold is a product of Yellow jacket Series 41 Manifolds with 2-1/2" Gauges color coded into Blue and Red, and it's equipped with color coded hoses; such as yellow, red and blue. The purpose of the pressure manifold is to achieve accurate pressure readings of the heat pump when it's under operating conditions. The High pressures are to be read from the 'Red' colored gauge and it's rated up to 500psi. This gauge is known as the "high pressure side". The T-type temperature probes were to be installed at the inlet and outlet of the ground loop side of the evaporator, whereas the K-type temperature probes were to be installed in the refrigerant loop at the following locations: the inlet of the evaporator, the outlet of the evaporator, the inlet of the condenser, and the outlet of the condenser. Before the temperature probes could be installed, ¼ inch pipe thread tees had to be fitted at each of the desired locations mentioned previously. To accurately visualize how far downward the temperature probes would cross the refrigerant flow area, a spare probe was twisted into a spare tee. The installed *T-type* thermocouples at the water-side inlet and outlet of the evaporator

have an accuracy of +/- 0.25°C, whereas the *K-Type* thermocouples at all refrigerant side have an accuracy of +/- 0.75°C. Locations of these thermocouples are shown in Fig. (**4**). A thermostatic expansion valve (TXV) was used in the heat pump loop and a standard rotameter was used in the geothermal water side of the loop to measure the flow rate. The type of compressor used in the heat pump is a hermetic rotary compressor with a rated electrical horsepower capacity of 0.5 hp.

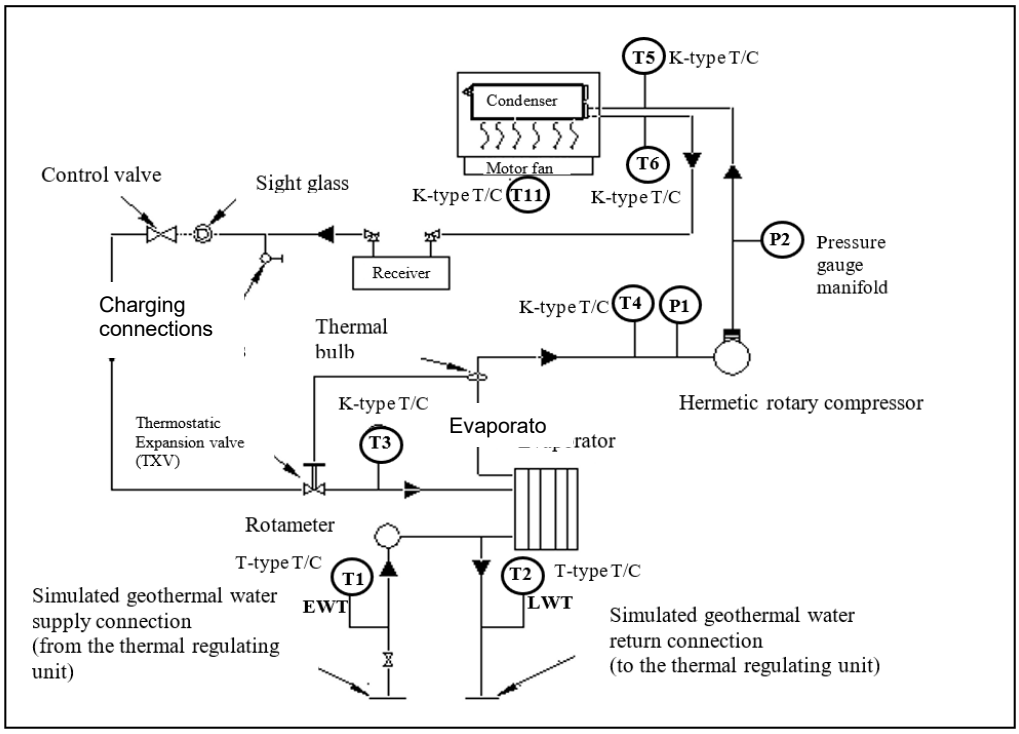

Figure 4: A schematic diagram showing flow diagram and instrumentations' locations of the GHP simulator used in this investigation.

The GHP simulator operates on a vapor-compression refrigeration cycle, represented by the theoretical temperature-entropy (T-s) diagram in Fig. (**5**). In this cycle, superheated vapor exits the evaporator at state (1) after absorbing heat (Q_L) from the temperature-controlled water bath (Sentra™ unit, Fig. (**3**)), which emulates a stable ground temperature. Process (1)–(2) represents isentropic compression, where electrical work input (W_{in}) increases refrigerant pressure and temperature. Process (2)–(3) denotes isobaric heat rejection in the condenser, where heat (Q_H) is transferred to the ducted airstream, resulting in condensation to saturated liquid at state (3). Process (3)–(4) is an isenthalpic throttling process through an expansion valve (capillary tube), causing a significant pressure drop. Finally, process (4)–(1) represents isobaric evaporation in the plate heat exchanger, where the refrigerant absorbs heat from the ground loop, completing the cycle by returning to state (1), as shown in Fig. (**5**). The cycle repeats continuously, enabling sustained heat absorption from the simulated ground loop via the evaporator and consistent heat rejection to the air duct system across the condenser. The designed lab-scale GHP experimental simulator closely replicates the thermodynamic operation of an actual geothermal heat pump, thereby providing critical insights and understanding into the anticipated performance of full-scale systems, potentially for the TBRHSC complex, under varied operating conditions.

3. Experimental Results and Discussion

3.1. Ground Temperature Profile

The sizing and configuration of a geothermal heat exchanger, normally the major component in an actual geothermal heat pump system, are critically dependent on the local soil's thermophysical properties, including thermal conductivity, thermal diffusivity, ground temperature, and moisture content. Reliance on estimated charts

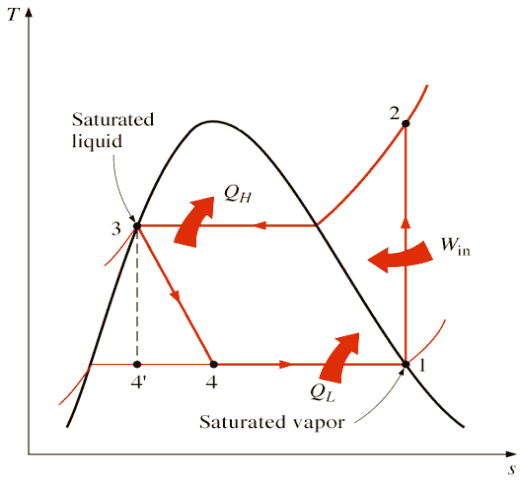

Figure 5: The theoretical T-s diagram for a heat pump cycle.

or predictive correlations for these parameters can lead to significant system oversizing or undersizing, resulting in either excessive capital costs or an inability to meet thermal demand. A more accurate and feasible design methodology is to base the system on experimentally determined geothermal properties, in this study it is the ground temperature profile. The variation of ground temperature with depth were experimentally obtained, from the main author's separate research phase I (2007-2009) of this work [26] (Fig. **6**), using a geothermal logging probe in a 100m deep borehole installed at the Goldcorp-Musselwhite gold mine, north of Thunder Bay, Northwestern Ontario. Fig. (**7**) shows the 9 locations of the installed thermocouples, namely, at 0.3m, 1m, 5m, 10m, 30m, 50m, 70m, and 95m. Table **1** [26] shows that the average ground temperature profile at the Goldcorp-Musselwhite mine site, during January—the coldest month of the year. The ground temperature profile provided detailed insights. It increases sharply within the upper soil strata but begins to stabilize and slightly decrease

Figure 6: Photographs showing the installation process of the borehole and geothermal logging station at Goldcorp-Musselwhite mine north of Thunder Bay, Northwestern Ontario (a separate research-phase I 2007-2009 of this project) [26].

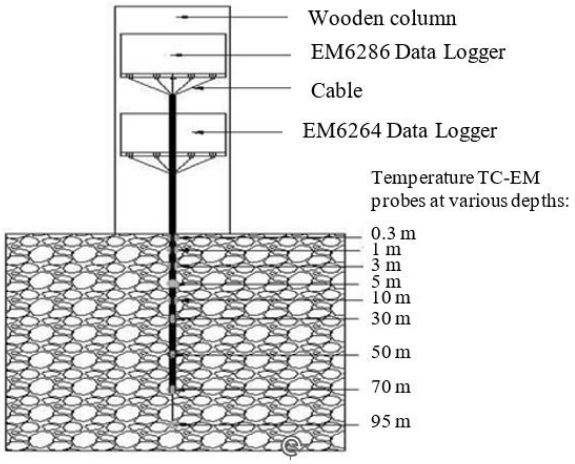

Figure 7: Temperature probes configuration in the borehole installed in the first phase of this project 2007-2009 [26] at Goldcorp-Musselwhite mine north of Thunder Bay, Northwestern Ontario.

beyond a depth of approximately 5 meters. Specifically, the temperature declines from 6.3°C at 5 m to 5.8°C at 10 m, remaining constant thereafter at greater depths. Based on this ground temperature profile, a preliminary design recommendation is to install the ground-loop heat exchanger of the GHP system near the 5-meter depth. This configuration would capture the warmest accessible subsurface temperatures while avoiding the incremental cost and complexity associated with deeper drilling.

Table 1: Averaged ground temperature, $T_{g,min}$, at Goldcorp-Musselwhite mine, north Thunder Bay, Northwestern Ontario-*Project Phase I* [26].

Depth (m)	Average $T_{g,min}$ Temperature (°C/°F)
1	1.2/34.2
3	5.4/41.7
5	6.3/43.3
10	5.8/42.4
30	4.5/40.1
50	3.9/39.0
70	3.9/39.0
95	4.0/39.2

3.2. Experimental Results of the GHP Simulator

Three experimental runs were conducted, with the independent variable set as the entering water temperature (EWT), representing the ground temperatures (i.e. the geothermal source temperature), on the simulated ground-loop side of the evaporator, successively fixed at an average EWT of 5°C, 10°C, and 15°C. Throughout all tests, the water volumetric flow rate was maintained at a constant 500 L/h — a mid-range value selected to balance thermal exchange efficiency and pumping power. Prior to each run, instrumentation including a Yello Jacket pressure manifold with dual K-type thermocouple readers, a hot-wire air-velocity meter, and two inline power meters (for the compressor and fan) were connected and verified. The entering water temperature was varied using the temperature-controlled water bath unit (i.e. the thermal regulator, Sentra™). Upon stabilization of the target EWT and flow conditions, key parameters—such as temperature, suction and discharge pressures, air velocity, and electrical power inputs—were recorded at two-minute intervals over a 30-minute duration. This procedure was repeated for each remaining EWT setpoint, yielding three complete datasets for performance analysis. The measurements results are shown in Table **2A**- **2C**.

Table 2A: Experimental results of the operating conditions (at a simulated geothermal water flow of 500 l/h) in the GHP simulator.

Time [min]	EWT T1 [°C]	LWT T2 [°C]	Evap In T3 [°C]	Evap Out T4 [°C]	Cond In T5 [°C]	Cond Out T6 [°C]	Duct Average T11 [°C]	Comp In P1 [kPa]	Comp Out P2 [kPa]	Duct Airflow [ft/min]
0	5.3	4.9	13.9	13.9	21.7	20.3	24.5	446	446	0
2	5.2	4.7	-0.3	1	70.2	44.9	36.6	322	1308	90
4	5.2	4.3	-1.5	1.5	72.8	46.4	38.2	315	1363	90
6	5.1	4.1	-1.1	1	74.9	46.9	38.9	315	1370	90
8	5.1	4.2	-1	2.3	76.4	47.2	39.2	315	1370	90
10	5.0	4.2	-0.8	2.6	77	47.5	39.4	315	1370	100
12	5.2	4.2	-0.6	3	78.1	47.6	39.7	315	1377	100
14	5.1	4.4	-0.5	3.1	78.6	47.6	39.7	315	1377	100
16	5.1	4.2	-0.6	3.2	79.3	47.7	39.7	315	1377	100
18	5.1	4.2	-0.7	3.2	79.9	47.7	39.8	315	1377	100
20	5.1	4.3	-0.7	3	80.7	47.7	39.9	315	1377	100
22	5.1	4.3	-0.5	3.1	81	48	40.0	315	1377	100
24	5.1	4.4	-0.5	3.2	81	48.2	39.9	315	1377	100
26	5.2	4.4	-0.5	3.3	81.5	48.4	40.1	315	1377	100
28	5.2	4.2	-0.5	3.5	81.5	48.1	40.1	315	1377	100
30	5.2	4.3	-0.5	2.7	81.5	48.63	40.2	315	1377	100

Table 2B: Experimental results of the operating conditions (at a simulated geothermal water flow of 500 l/h) in the GHP simulator.

Time [min]	EWT T1 [°C]	LWT T2 [°C]	Evap In T3 [°C]	Evap Out T4 [°C]	Cond In T5 [°C]	Cond Out T6 [°C]	Duct Average T11 [°C]	Comp In P1 [kPa]	Comp Out P2 [kPa]	Duct Airflow [ft/min]
0	10.3	10.8	15.0	17.5	45.2	30.4	28.6	391	1377	0
2	10.0	9.2	4.2	8.7	76.7	49.5	33.9	363	1411	100
4	10.0	8.9	3.5	8.7	80.1	50.4	40.6	363	1480	100
6	10.0	8.8	3.5	8.4	82.9	51.1	41.6	356	1480	100
8	9.9	8.7	3.5	8.6	85.2	51.4	41.8	356	1480	100
10	9.9	8.7	3.7	8.6	87.0	51.8	42.2	356	1487	100
12	9.9	8.8	3.6	8.4	88.4	51.8	42.4	356	1501	100
14	9.8	8.7	3.7	8.6	89.7	50.8	42.6	356	1515	100
16	9.8	8.9	3.8	8.4	90.5	52.3	42.8	356	1515	100
18	9.8	8.8	3.8	8.5	91.3	52.1	42.9	356	1515	100
20	9.9	9.0	3.8	8.3	91.7	51.9	43.0	356	1515	100
22	9.9	8.9	4.0	8.0	91.8	52.1	43.0	356	1515	100
24	9.9	8.8	4.0	8.2	92.1	52.0	43.0	356	1515	100
26	9.9	8.8	3.6	7.8	92.3	52.3	43.1	356	1515	100
28	9.8	8.8	3.6	7.8	92.7	53.7	43.1	356	1515	100
30	9.8	8.8	3.7	7.9	92.5	50.9	43.2	356	1515	100

Table 2C: Experimental results of the operating conditions (at a simulated geothermal water flow of 500 l/h) in the GHP simulator.

Time [min]	EWT T1 [°C]	LWT T2 [°C]	Evap In T3 [°C]	Evap Out T4 [°C]	Cond In T5 [°C]	Cond Out T6 [°C]	Duct Average T11 [°C]	Comp In P1 [kPa]	Comp Out P2 [kPa]	Duct Airflow [ft/min]
0	15.1	15.3	15.5	19.1	46.8	35.5	29.1	432	1308	0
2	14.7	13.5	7.9	11.3	85.0	53.3	37.6	412	1549	100
4	14.6	13.1	7.4	11.7	89.4	54.0	43.7	405	1549	100
6	14.6	13.0	7.3	11.8	92.5	54.4	44.4	405	1549	100
8	14.6	13.0	7.4	12.3	95.5	55.0	44.9	405	1618	100
10	14.6	13.1	7.5	12.4	96.4	55.3	45.3	405	1618	100
12	14.5	13.2	7.5	12.9	99.1	55.4	45.4	405	1618	100
14	14.6	13.2	7.4	12.4	100.4	55.7	45.5	405	1618	100
16	14.6	13.3	7.5	12.9	100.1	55.9	45.7	405	1618	100
18	14.6	13.3	7.6	13.1	102.6	56.0	45.8	405	1618	100
20	14.6	13.3	7.7	12.4	103.3	55.8	45.9	405	1653	100
22	14.6	13.3	7.6	12.2	104.0	55.9	46.1	405	1653	100
24	14.7	13.4	7.7	12.2	104.4	56.1	46.1	405	1653	100
26	14.6	13.3	7.8	11.9	105.1	56.5	46.1	405	1653	100
28	14.6	13.3	7.8	12.4	105.2	56.3	46.2	405	1653	100
30	14.6	13.3	7.7	12.4	105.6	56.5	46.2	405	1653	100

As graphically shown in Fig. (**8**), the supply air temperature rises rapidly following system start-up, with each tested condition achieving approximately 90% of its peak value within the first 4 to 5 minutes. A consistent thermal gain is observed, where each 5°C increase in entering water temperature (EWT) yields an additional ~3°C rise in useful supply air temperature. After approximately 10 minutes, the temperature gradients plateau, indicating that the system has achieved a thermal steady state. Fig. (**8**) thus confirms that elevated EWTs directly enhance heating capacity, a fundamental relationship that informs the ground-loop heat exchanger design and sizing strategy.

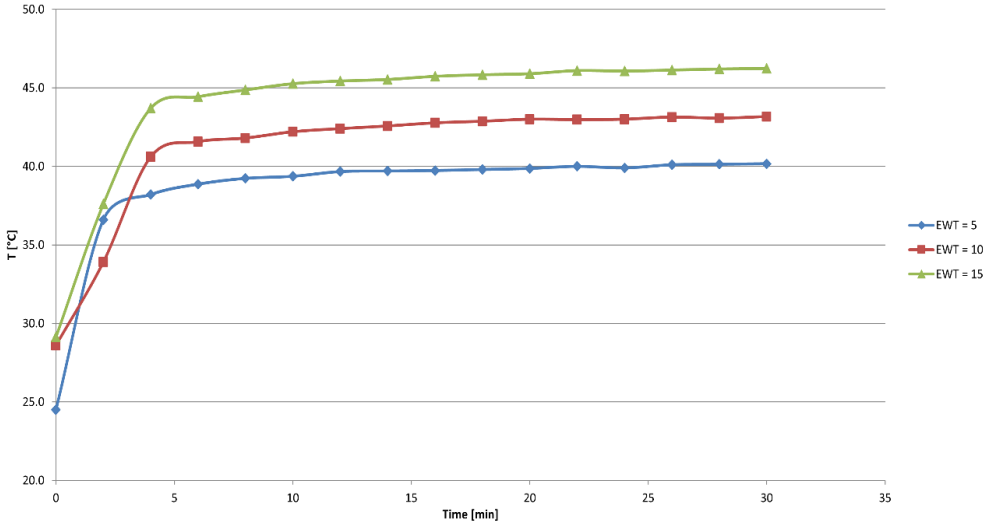

Figure 8: GHP average duct air temperature for variable EWT at constant water flow rate of 500 l/h.

Table 3A: Experimental results of the operating conditions (at a simulated geothermal water flow of 200 l/h) in the GHP simulator.

Time [min]	EWT T1 [°C]	LWT T2 [°C]	Evap In T3 [°C]	Evap Out T4 [°C]	Cond In T5 [°C]	Cond Out T6 [°C]	Duct Average T11 [°C]	Comp In P1 [kPa]	Comp Out P2 [kPa]	Duct Airflow [ft/min]
0	5.6	5.6	15.5	21.6	24.1	26.7	69.2	460	474	0
2	5.6	4.2	-7.5	7.9	46.4	36.8	91.3	267	998	100
4	5.7	4.2	-3.2	7.1	54.9	39.9	99.7	274	1101	100
6	5.6	4.2	-1.7	6.4	62.1	40.7	104.4	287	1136	100
8	5.7	4.3	-1.2	6.5	69.2	42.4	107.0	294	1170	100
10	5.7	4.3	-0.3	6.8	71.4	42.7	108.7	294	1170	100
12	5.5	4.5	-0.5	6.2	75.6	42.8	110.0	301	1204	100
14	5.6	4.4	-0.6	6.1	78.9	42.9	111.2	301	1204	100
16	5.5	4.4	-0.5	6.2	81.9	43	111.5	301	1204	100
18	5.5	4.6	-0.3	6.3	84.5	43.3	112.1	301	1204	100
20	5.6	4.5	0.2	6.2	86.3	42.4	113.1	301	1204	100
22	5.6	5.0	0.1	6.3	88.6	43.6	113.3	301	1204	100
24	5.6	4.8	0.5	6.3	90	43.7	113.6	301	1204	100
26	5.6	5.2	0.1	6.1	91.6	43.8	114.0	301	1204	100
28	5.6	5.2	-0.1	6	92.4	44	114.4	301	1204	100
30	5.6	4.8	0.2	6.2	94.5	44.3	114.3	301	1204	100

Table 3B: Experimental results of the operating conditions (at a simulated geothermal water flow of 400 l/h) in the GHP simulator.

Time [min]	EWT T1 [°C]	LWT T2 [°C]	Evap In T3 [°C]	Evap Out T4 [°C]	Cond In T5 [°C]	Cond Out T6 [°C]	Duct Average T11 [°C]	Comp In P1 [kPa]	Comp Out P2 [kPa]	Duct Airflow [ft/min]
0	5.7	5.7	33.8	12.2	67.4	34	28.0	418	446	0
2	5.5	5.2	6.3	4.1	79.8	42.3	37.2	308	1204	100
4	5.5	5.2	0.2	5.3	86.8	43.3	37.9	308	1204	100
6	5.3	4.9	-0.4	5.7	89.3	43.4	38.1	308	1204	100
8	5.3	4.7	0	5.9	90.6	43.9	38.2	308	1204	100
10	5.3	4.7	0.1	5.9	92.3	44	38.2	308	1204	100
12	5.4	5.0	0.1	6	93.7	44	38.3	308	1204	100
14	5.4	4.9	0.2	6.1	94.3	44	38.3	308	1239	100
16	5.5	4.9	0.1	6.3	95.2	44.2	38.3	308	1239	100
18	5.6	5.1	0.3	6.1	95.9	44.5	38.3	308	1239	100
20	5.6	5.0	0.1	6.2	96.7	44.5	38.4	308	1239	100
22	5.6	5.1	0.4	6.4	97.1	44.1	38.4	308	1239	100
24	5.6	5.1	0.3	6.2	97.8	44	38.4	308	1239	100
26	5.6	5.0	0.3	6.3	98	44.1	38.4	308	1239	100
28	5.8	5.1	0.1	6.2	98.3	44.1	38.4	308	1239	100
30	5.7	5.0	0.2	6.4	98.8	44.2	38.3	308	1239	100

In the second experimental settings, the entering water temperature (EWT) was maintained at an average temperature of 5˚C, while the simulated geothermal water flow rate was varied from 200 L/h to 600 L/h. The measurements results are shown in Table **3A**- **3C**.

Table 3C: Experimental results of the operating conditions (at a simulated geothermal water flow of 600 l/h) in the GHP simulator.

Time [min]	EWT T1 [°C]	LWT T2 [°C]	Evap In T3 [°C]	Evap Out T4 [°C]	Cond In T5 [°C]	Cond Out T6 [°C]	Duct Average T11 [°C]	Comp In P1 [kPa]	Comp Out P2 [kPa]	Duct Airflow [ft/min]
0	5.4	4.6	13.6	15.8	46.1	29.3	28.2	412	446	0
2	5.4	4.2	12.4	4.1	74.2	35.2	36.7	301	1170	100
4	5.3	5.0	-0.9	4.6	86.9	42.6	37.3	301	1170	100
6	5.3	4.9	-0.7	4.8	90.6	43	37.5	301	1204	100
8	5.3	4.9	-0.9	5	91.5	42.9	37.4	301	1204	100
10	5.3	4.9	-0.9	5.1	93.1	43	37.5	301	1204	100
12	5.3	4.9	-0.7	4.8	93.9	42.9	37.5	301	1204	100
14	5.3	5.0	-1.1	4.7	94.2	43.1	37.7	301	1204	100
16	5.3	5.0	-1.1	5.1	95.4	43	37.6	301	1204	100
18	5.3	5.0	-0.8	5.6	96.3	43.1	37.7	301	1204	100
20	5.3	5.0	-0.7	5.3	96.6	42.9	37.7	301	1204	100
22	5.3	4.9	-1.1	5.1	96.9	43	37.7	301	1204	100
24	5.3	5.0	-1	5.1	97.4	42.9	37.7	301	1204	100
26	5.3	5.0	-0.9	5	97.7	42.8	37.9	301	1204	100
28	5.3	5.0	-1	5.1	98	42.6	37.9	301	1204	100
30	5.3	5.0	-1	5.1	98.6	43.1	38.1	301	1204	100

The results are presented in Fig. (**9**). In all tested cases, the air temperature rises rapidly during the initial five minutes, after which the curves plateau as the system approaches steady state. Increasing the flow rate from 200 L/h to 400 L/h elevates the quasi-steady air temperature by approximately 2°C and shortens the warm-up transient, indicating enhanced evaporator-side heat extraction. However, a further increase to 600 L/h yields no additional thermal gain, as the corresponding temperature profiles converge. This result demonstrates a point of diminishing returns, where higher mass flow no longer translates to appreciable heating output but would incur increased pumping power in a full-scale installation. Consequently, for the laboratory setup at the selected EWT, a flow rate of approximately 400 L/h appears optimal, providing near-maximum outlet air temperature of approximately 38°C while avoiding unnecessary energy expenditure for fluid circulation. Another important result obtained from these tests is the $\mathrm{COP_{sys}}$ (coefficient of performance for the GHP system), defined as the ratio between rate of heat delivered to the total input power of the GHP simulator. It is the measure of how efficient the GHP is in a heating mode and is given by the equation:

$$\mathrm{COP_{sys}} = \frac{q_H}{W_{in}} = \frac{\dot{m}_{air}\, C_P (T_6 - T_5)}{\dot{W}_{comp} + \dot{W}_{fan}} \quad (1)$$

Where, $\dot{m}_{air}$ is the mass flow rate of air (kg/s), C_p is the specific heat of air (kJ/kg.°K), T_6 is the average duct temperature (°C), and T_5 is the average room temperature at that moment (°C). These variables determine the amount of heat that is delivered from the condenser. While W_{comp} and W_{fan} are the amount of electrical power being used by the compressor and the fan to run the system. Some variables that stay constant are the specific heat of air, mass flow rate produced by the fan and the room temperature.

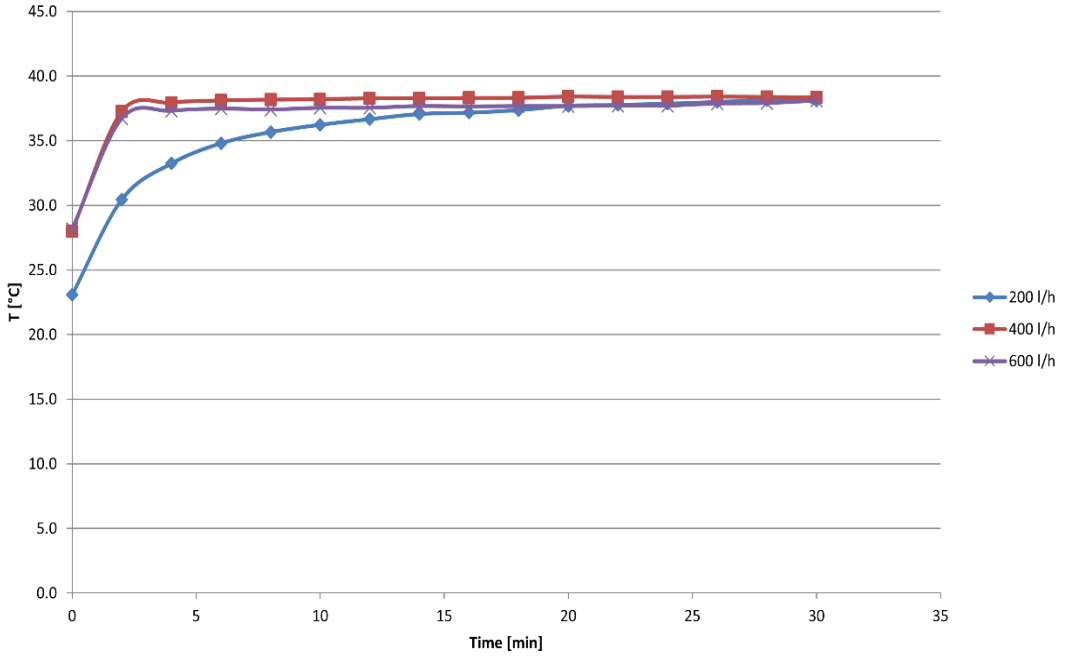

Figure 9: GHP average airflow temperature delivered by the duct system for variable water flow rate at a constant EWT of 5°C.

As presented in Table **4**, progressively increasing the simulated ground-loop water temperature entering the evaporator from 5°C to 10°C and then to 15°C results in a corresponding rise in supply air temperature (38.5°C, 41.1°C, and 44.0°C, respectively) and an improvement in the system's coefficient of performance (COP) from 8.73 to 8.90 and finally to 9.36. These experimentally simulated results confirm that a warmer ground source simultaneously augments the heating capacity and improves the performance of the GHP by reducing compressor work. This trend agrees with the experimental study given in reference [9]. It should be noted that the high COP values achieved under controlled laboratory conditions represent an optimistic upper bound, and actual field performance at TBRHSC would likely be lower due to system losses and operational variability.

Table 4: The results of the average COP_{sys} and the average air supply temperatures by the GHP's duct system at different simulated EWT.

Entering Simulated Ground Water Temperature T_{EWT}(°C)	$T_{air,\ duct}$ (°C)	COP_{system}
5	38.5	8.73
10	41.1	8.90
15	44.0	9.36

4. Conclusions

The building sector, particularly space heating for residential and institutional complexes, represents a dominant fraction of Canada's primary energy consumption and a major source of greenhouse gas (GHG) emissions—a challenge amplified by Canada's cold climate. This is especially critical in regions like Thunder Bay, where extreme winter conditions impose substantial heating demands, making building operations a principal contributor to local emissions. Geothermal heat pumps (GHP) offer a highly efficient technological pathway, leveraging the stable thermal energy of the subsurface for space conditioning. By utilizing the ground as a heat source in winter and a thermal sink in summer, GHPs can reduce building energy use for heating and cooling by an estimated 25–50% compared to conventional systems. This positions them as a promising decarbonization solution for large-scale applications, as proposed for the Thunder Bay Regional Health Sciences Centre (TBRHSC), a critical healthcare facility and one of the city's most energy-intensive infrastructures. However, a significant

research gap exists regarding region-specific performance data and operational understanding of GHPs in Northwestern Ontario. This study addresses that gap by experimentally characterizing a lab-scale GHP system using actual subsurface temperature profiles from a local site. A fully instrumented GHP simulator was used to evaluate system performance under a controlled range of operating conditions. Key performance metrics from these simulations were presented and analyzed. Experimental results showed that the GHP's supply air temperature rises rapidly upon start-up. Thermal steady state was typically achieved within 10 minutes. Furthermore, progressively increasing the EWT from 5°C to 15°C resulted in a corresponding increase in both supply air temperature and the system's coefficient of performance (COP). The insights derived from this experimental work establish a foundational understanding for future high-fidelity numerical simulations to model and optimize a large-scale GHP system for potential application at the TBRHSC in extreme cold climate in Northwestern Ontario. Future work of this project may focus on performing a comprehensive energy, economic, and GHG emissions analyses and optimization of a proposed large-scale hybrid solar PV-GHP system integration to the TBRHSC facility in Northwestern Ontario.

Conflict of Interest

The authors declare no conflict of interest.

Funding

The study received no financial support.

Acknowledgents

The first phase of this project (2007-2009) was supported by Goldcorp Canada Limited-Musselwhite Gold Mine, whose financial and in-kind supports were greatly appreciated. This mainly included the drilling and installation (first phase) of the on-site boreholes and geothermal logging stations setups and arranging for the main author's Lakehead University-Mechanical Engineering graduate students' (Ayman Abdulrahman and Azib F. Khan) and undergraduate students' (Michael Nelson, Sunny Lim, and Roshan Perera) regular field trips related to acquiring and compiling geothermal data at the site. Acknowledgements also go to Esteban figueroa, Nuri Himidi, Tim Sanford, and others from Musselwhite Mine for their kind support and insightful technical suggestions. The main author of this work would also like to acknowledge M. Nelson, S. Lim, R. Perera, M. Murdoch, P. Auffret, and Hubbard Mechanical for their initial technical assistance related to the GHP simulator. Acknowledgement also goes to Ryan Sears and Darin Pretto with the TBRHSC for their recent invitation related to Dr. Basel I. Ismail's (main author of this work) visit and tours to the TBRHSC facility for a proposal discussion related to future potential research exploration for applying a hybrid solar-geothermal heat pump system for heating the large-scale TBRHSC facility located in extreme cold climate of Northwestern Ontario.

References

[1] Bagherian MA, Mehranzamir K. A comprehensive review on renewable energy integration for combined heat and power production. Energy Convers Manag. 2020; 224: 113454. https://doi.org/10.1016/j.enconman.2020.113454

[2] Natividad LE, Benalcaraz P. Hybrid renewable energy systems for sustainable rural development: perspectives and challenges. Energy Syst. 2023; 16: 1328. https://doi.org/10.3390/en16031328

[3] Banister C, Hayne H, Pellissier M. Renewables for decarbonization and resiliency for remote and arctic communities in Canada: technical and logistical challenges and review of installation projects. In: ASHRAE and SCANVAC HVAC Cold Climate Conference; 2023 Mar 6-8; Marriott Anchorage Downtown, Anchorage, Alaska, USA.

[4] Violante AC, Donato F, Guidi G, Proposito M. Comparative life cycle assessment of the ground source heat pump vs air source heat pump. Renew Energy. 2022; 188: 1029-37. https://doi.org/10.1016/j.renene.2022.02.075

[5] Wang X, Zhan T, Liu G, Ni L. A field test of medium-depth geothermal heat pump system for heating in severely cold region. Case Stud Therm Eng. 2023; 48: 103125. https://doi.org/10.1016/j.csite.2023.103125

[6] Han J, Cui M, Chen J, Lv W. Analysis of thermal performance and economy of ground source heat pump system: a case study of the large building. Geothermics. 2021; 89: 101929. https://doi.org/10.1016/j.geothermics.2020.101929

[7] Ochsner K. Geothermal heat pumps: a guide for planning and installing. Trowbridge, Wiltshire, England: Cromwell Press; 2008.

[8] Wang F, You T. Comparative analysis on the life cycle climate performance of ground source heat pump using alternative refrigerants. Case Stud Therm Eng. 2023; 42: 102761. https://doi.org/10.1016/j.csite.2023.102761

[9] Harjunowibowo D, Omer SA, Riffat SB. Experimental investigation of a ground-source heat pump system for greenhouse heating-cooling. Int J Low-Carbon Technol. 2021; 16: 1529-41. https://doi.org/10.1093/ijlct/ctab052

[10] Skye HM, Wu W. Experiments and exergy analysis for a carbon dioxide ground-source heat pump in cooling mode. Int J Refrig. 2021; 131: 920-37. https://doi.org/10.1016/j.ijrefrig.2021.08.018

[11] Gao W, Masum S, Qadrdan M, Thomas HR. A numerical study on performance efficiency of a low-temperature horizontal ground-source heat pump system. Energy Build. 2023; 291: 113137. https://doi.org/10.1016/j.enbuild.2023.113137

[12] Zhang L, Feng G, Li A, Huang K, Chang S. Comprehensive evaluation and analysis of a nearly zero-energy building heating system using a multi-source heat pump in severe cold region. Build Simul. 2023; 16: 1949-70. https://doi.org/10.1007/s12273-023-0990-8

[13] Kapicioglu A. Energy and exergy analysis of a ground source heat pump system with a slinky ground heat exchanger supported by nanofluid. J Therm Anal Calorim. 2022; 147: 1455-68. https://doi.org/10.1007/s10973-020-10498-0

[14] Eicker U. Energy efficient buildings with solar and geothermal resources. Chichester, UK: Wiley; 2014. https://doi.org/10.1002/9781118707050

[15] Sah SK, Murugesan K, Rajasekar E. Experimental comparison of first-law analysis of peak hour operation of GSHP system under optimized conditions. Appl Therm Eng. 2025; 253: 124525. https://doi.org/10.1016/j.applthermaleng.2024.124525

[16] Sah SK, Murugesan K, Rajasekar E. Experimental investigation of energy-saving potential of ground source heat pump during peak hour operations. J Therm Sci Eng Appl. 2024; 16: 021010-1. https://doi.org/10.1115/1.4064138

[17] Salhein K, Salheen SA, Annekaa AM, Hawsawi M, Alhawsawi EY, Kobus CJ, et al. A comprehensive review of geothermal heat pump systems. Processes. 2025; 13: 2142. https://doi.org/10.3390/pr13072142

[18] Acar B. Experimental investigation on the effect of soil type on ground source heat pumps performance and energy consumption. Therm Sci. 2020; 24(2A): 843-52. https://doi.org/10.2298/TSCI181216028A

[19] Rosen MA, Koohi-Fayegh S. Sustainable heating and cooling using the ground. Chichester, UK: Wiley; 2017.

[20] Kavanaugh S, Rafferty K. Geothermal heating and cooling: design of ground-source heat pump systems. ASHRAE Research Project RP-1674. Atlanta, GA, USA: ASHRAE; 2014.

[21] El Haj Assad M, AlMallahi MN, Ramadan A, Awad MA, Rejeb O, AlShabi M. Geothermal heat pumps: principles and applications. In: 2022 Advances in Science and Engineering Technology International Conferences (ASET). IEEE 2022; ASET53988.2022:9734907.

[22] Sarbu I, Sebarcievici C. Ground-source heat pumps: fundamentals, experiments and applications. Oxford, UK: Elsevier; 2016. https://doi.org/10.1016/B978-0-12-804220-5.00005-9

[23] Feng H, Xu H, Feng H, Gao Y. Numerical simulation and experimental study of medium and deep ground source heat pump systems in a cold and arid region. Case Stud Therm Eng. 2024; 64: 105473. https://doi.org/10.1016/j.csite.2024.105473

[24] Qu S, Han J, Sun Z, Yin R, Ji R, Chai C. Study of operational strategies for a hybrid solar-geothermal heat pump system. Build Simul. 2019; 12: 697-710. https://doi.org/10.1007/s12273-019-0519-3

[25] Energy Conservation and Demand Management 2024 – 5 Year Plan [Internet]. 2024 [cited 2025 Nov 25]. Available from: https://tbrhsc.net/wp-content/uploads/2024/06/Energy-Usage-Conserv-Plan-2024.pdf

[26] Ismail BI, Abdelrahman A, Khan AF, Bujold J. Performance characteristics of a geothermal heat pump system under simulated ground thermal conditions of Goldcorp-Musselwhite Mine's site, Ontario, Canada. In: 3rd International Conference and Exhibition on Clean Energy (ICCE2014); 2014 Oct 20-22; Quebec City, Quebec, Canada.